Modeling Ambient Light in Stratified Waters for Underwater Optical Wireless Communication

Tharuka Govinda Waduge
Department of EEE
Auckland University of Technology
Auckland, New Zealand
tharuka.waduge@autuni.ac.nz

Boon-Chong Seet
Department of EEE
Auckland University of Technology
Auckland, New Zealand
boon-chong.seet@aut.ac.nz

Kay C. Vopel
Department of Environmental Science
Auckland University of Technology
Auckland, New Zealand
kay.vopel@aut.ac.nz

***Abstract*— Underwater optical wireless communication (UOWC) is a research field that has gained popularity with the advent of unmanned underwater vehicles (UUV). Its utilization is crucial in marine industries engaging in sustainable alternatives for food and energy security. Despite its potential to meet the high data rate and low latency requirements of underwater video transmission for UUV operations, UOWC links are affected by the inhomogeneous light attenuation underwater and the presence of sunlight within the photic region. This work investigates how the underwater light field distribution could be modeled for eight different stratified water columns. The results show a significant penetration of the blue-green solar spectra in both clear and coastal waters, significantly increasing ambient noise and thus challenging the common belief that blue-green spectrum is the most suitable for underwater communication.**

Keywords*— *Underwater optical wireless communication, stratified waters, mobile communication, solar noise.

I. INTRODUCTION

With the growing demand for food and energy resources, and the exacerbating climate conditions, scientists across the world are exploring new ways to venture into the oceans for sustainable agricultural and industrial alternatives. Collectively termed as the "Blue Economy", marine ventures such as aquaculture farms, carbon-capture facilities, and the provision of renewable energy (wind, wave, solar) are some examples of ocean-based economic activities that are expected to reach 3-trillion USD per-annum by the year 2030 [1]. Partners of blue economy activities have recognized the importance of automating tasks, such as monitoring fish-health and biofouling inside aquaculture enclosures, conducting seabed surveys, or inspecting and repairing underwater pipelines and cables, using unmanned underwater vehicles (UUV), which offer better efficiency, accuracy and safety than human divers, while achieving similar or better economic outcome [2]–[5]. These tasks may be conducted by a single UUV or by swarms, e.g., a series of miniature biomimetic robots [6]–[8]. Tethers are the most common approach for communication between operators and UUVs. However, they limit the UUV's manoeuvrability and range, due to drag, tension, and finite length, and are prone to costly damage, entanglement and breakage, and pose many challenges towards swarming operations [4], [9], [10]. Such cables are again easily damaged and subject to biofouling during long-term deployments. The alternatives to tethers are wireless communication using acoustic, radio frequency (RF), magnetic, or optical signals.

Acoustic underwater communication, the most mature form, dates to the late 1980s. However, acoustic links operate in the audible-ultrasound range (~ 20 kHz), resulting in low bandwidths and data rates in the tens of kbps, and are insufficient to transmit multimedia [11]. On the other hand, the use of RF is limited to extremely low-frequency ranges due to the severe attenuation of the higher spectrum by high conductivity seawater, and this requires large antennas and transmission power, posing challenges for compact UUVs with limited energy budget [11]. Magnetic Induction (MI) for underwater communication is based on inducing signals between coils of wire. The technology is relatively new, with limited transmission range and alignment challenges between coils, complicating mobile scenarios [12].

In contrast, underwater optical wireless communication (UOWC) employs specific wavelengths of light within the visible range of the electromagnetic spectrum, taking advantage of wavelengths that show the least attenuation across the light spectrum, and enabling high data rates exceeding 1 Gbps and transmission distances up to few hundred meters in point-to-point (P2P) configurations. For example, the authors in [13], [14] have showcased impressive data transmission rates of 16.4 Gbps (10 m range) and 12.4 Gbps (1.7 m range) using lasers. They have also achieved a 205 Mbps connection over a 10 m distance using blue light-emitting diodes (LEDs) [15]. However, UOWC faces challenges such as directionality, where light obstructed by objects like fish or debris may cause signal loss. In addition to this, environmental conditions such as ambient light, scattering, backscattering from suspended particles, and refraction with varying refractive indices along the propagation pathway deteriorate signal quality [11]. Nevertheless, these drawbacks may be overcome by improving signal adaptability, given its potential is underscored by the channel's high capacity, low latency and low cost-per-bit compared to the other wireless alternatives. For example, off-the-shelf components such as lasers, LEDs and photodiodes (PD) can be used to build high-frequency emitters and thus employ modulation and diversity schemes that enhance bandwidth and range, which is an advantage over acoustic or RF systems that require costly complex transducers [16].

As a step towards contributing to the adaptability of UOWC, this paper investigates in-depth the distribution of ambient light under realistic ocean stratification scenarios. This knowledge may be useful for UOWC within localized environments such as aquaculture farms, or renewable energy sites where the region of survey by UUV, or region of UOWC connectivity spans depths of the euphotic and disphotic zones.

II. Background

A. Basic Considerations for Mobile UOWC

A generic UOWC involves a transmitter generating photons that traverse water and are reconverted to electrical signals at the receiver. UOWC layers comprise subsystems coordinating for transmission. The data source, from a UUV's computer or camera, undergoes modulation, linking to a light source via a driving circuit, potentially using an optical amplifier and an instrument for beam control. At the receiver, photons are collected by lenses into a photodetector and then amplified, noise-filtered, demodulated into frames, and finally applied for the intended purpose.

Photon behavior underwater depends on the intrinsic and apparent optical properties of water (IOP and AOP, respectively) [11]. IOP, are influences on link that principally constitutes light absorption and scattering due to dissolved and particulate substances and ocean currents. AOP relates to physical parameters defining the optical beam's structure, tied to engineering choices like beam divergence angle and those defined by medium composition such as the reflectance. The combined IOP effects of absorption and scattering give rise to the signal attenuation as expressed in (1), where a portion of the signal energy is either converted to another energy form (chemical or heat) or is redirected away from the intended path; $c(\lambda)$ is the overall wavelength-dependent attenuation, which is the sum of absorption $a(\lambda)$ and scattering $b(\lambda)$ coefficients, at vacuum wavelength of light λ in nm.

$$c(\lambda) = a(\lambda) + b(\lambda) \quad (1)$$

The nominal values for c, of 0.056 m^{-1}, 0.15 m^{-1}, 0.305 m^{-1} and 2.17 m^{-1} are used for modeling pure seawater, clear ocean water, coastal ocean water, and turbid water in harbors, respectively [11], [17]. The classification by Jerlov [18], which is recognized as more appropriate for applications, identifies nine types of waterbodies: I, IA, IB, II, and III, which are clear oceanic waters; and 1C, 3C, 5C, and 7C, which are coastal waters of increasing turbidity [18]. Nevertheless, both classifications assume that the water body is homogeneous with depth, at a given location (Jerlov types are only accurate up to 10 m water depth assuming relative homogeneity in this layer [19]), which could be an issue for studying mobile UOWC scenarios where the parameters that influence signal could drastically change should the link travel through depths where the water quality has changed. This is evident in the derivation of absorption and scattering coefficients given in (2) and (3) which are the linear sum of its subcomponents, where w, $CDOM$, phy, and det denotes absorption and scattering by pure seawater, coloured dissolved organic matter (such as released from decaying organisms), phytoplankton (photosynthetic organisms), and detritus (organic and inorganic suspended particulates), respectively. The weightage of each is determined by the concentration present within that permissible locality. It is generally accepted that blue-green light is optimal for transmission in clear ocean water with a shift towards green-amber wavelengths in more turbid waters, as seen in Fig. 1.

$$a(\lambda) = a_w(\lambda) + a_{CDOM}(\lambda) + a_{phy}(\lambda) + a_{det}(\lambda) \quad (2)$$

$$b(\lambda) = b_w(\lambda) + b_{phy}(\lambda) + b_{det}(\lambda) \quad (3)$$

Beer-Lambert's law may then be used to model the loss of signal propagation for a distance d, given as (4), where I_t is the irradiance at the location of interest, and I_0 is the initial irradiance at the point of emission.

$$I_t = I_0 e^{-c(\lambda)d} \quad (4)$$

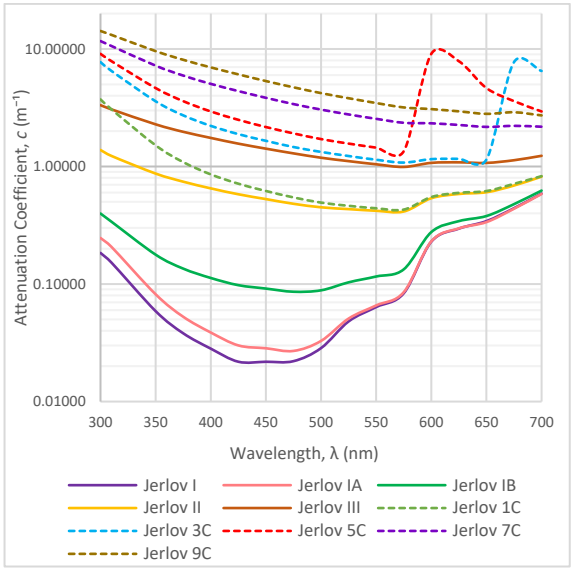

Fig. 1. Spectral attenuation distribution of Jerlov types.

However, the concentrations of these subcomponents in (2) and (3) are subject to variation due to:

1. The changing water quality surrounding a mobile UUV
2. The diel and/or seasonal changes.
3. The changing water quality surrounding a fixed UUV as currents change.

To study the UOWC performance in time-varying environments, we need to perform these tasks: (i) realistically estimate the downwelling light; (ii) identify the vertical variation in attenuation parameters; (iii) model the interactions between tasks (i) and (ii) with depth; and (iv) apply UOWC propagative models in this environment.

In this paper, we propose models and study the outcomes of tasks (i)-(iii), which in turn will build the stage for applying the propagative models in task (iv).

III. Time-Varying Environmental Influences

Established previously, quality of the wireless optical signal can deteriorate for two reasons: ambient light (from solar or lunar radiation) that increase optical noise and changing light attenuation due to changes in the concentrations of dissolved and suspended matter.

A. *Downwelling Ambient Light*

The level of radiance reaching the sea surface changes throughout the day depending on the Sun's azimuth and zenith angles, due to the Earth's axial tilt and elliptical orbit around the Sun, causing the penetrating light rays to be refracted at the air-water boundary., and is further impacted by cloud cover. This effect is significant even in some of the earliest investigations of the underwater light field in [20], and later in [21], where at a constant depth, the radiance was greatest when the receiver was directed towards the azimuth and zenith angles that corresponded to the refracted rays as per Snell's law. However, these directional characteristics are lost with increasing depth as the light field transforms progressively from the "sunny condition" near surface to a more diffuse distribution where ultimately, the peak radiance underwater occurs at a zenith angle of zero, where it has reached its asymptotic form [22].

Due to those reasons, accurate downwelling spectral distribution is difficult to obtain without in-situ measurements dependent on time and offshore location. However, the SPCTRAL2 model developed in [23] may be a robust alternative to estimate the spectra based on date, time and location (latitude and longitude), estimating accurately for the solar zenith and azimuth angles, and atmospheric parameters. In Fig. 2, it can be seen that the global spectral distribution (includes both direct and diffuse sunlight) is highest at the blue-green region of optical spectrum that also corresponds to the spectra with the most penetrative ability underwater [11], thus raising questions of how significant this could contribute as optical noise.

The influence of lunar spectral radiance on the other hand may be considered less significant due to the irradiation peaking at about 5 mW/m^2 shifting towards the orange-red spectrum for a full moon (which experience higher attenuation) [24]. However, despite having lesser information for modelling the lunar spectra, given the spectral distribution coincides with solar spectrum, it can be assumed that strategies that discriminate solar noise could apply to lunar noise also.

With respect to the availability of sunlight underwater, the ocean is divided into three zones. The euphotic zone is the uppermost section with an abundance of light and usually reaches a depth of about 200 m in clear waters. Beneath this is the disphotic zone, by which much of the yellow and red spectra have already been absorbed but blue-green spectra are still available. This is a few kilometers deep. Beyond this is the aphotic zone, by which all downwelling light has diminished [11].

B. *Stratified Oceans*

Ocean color sensors on earth-observation satellites such as the Sea-viewing Wide Field-of-view Sensor (Sea WiFS) and Ocean Color and Temperature Scanner have been used for a long time to monitor concentration distribution of chlorophyll-a [Chl-a] on the sea surface, the principal pigment in chlorophyll [25].

Given there is an abundance of sunlight closer to the surface, the chlorophyll concentration is primarily influenced by nutrient availability. However, below the photic zone, where sunlight penetration is limited, photosynthesis is constrained, leading to a decrease in chlorophyll concentration. Within the transitional zone between sunlit, nutrient-poor waters and dark, nutrient-rich waters, a phenomenon known as the deep chlorophyll maximum (DCM) is observed. The DCM represents a peak in chlorophyll concentration, attributed to an optimal balance between light and nutrient conditions. The depth of this maximum typically falls within the range of 20 to 120 m, contingent on the surface concentration of chlorophyll [26]. The consistency of this phenomenon has led to the development of models, correlating with empirical data, for the relative Gaussian distribution of [Chl-a] along a vertical column of water and is presented in [25]. Furthermore, these models are consistent for oceans that are stratified, a very common occurrence, where the depth layers do not mix, and thus enabling parameterization [26].

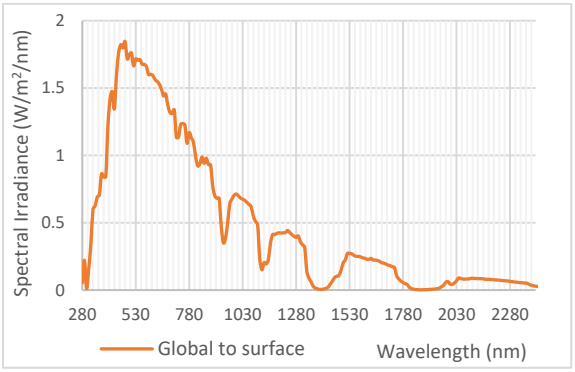

Fig. 2. Spectral distribution of global irradiance generated for a clear summer day in Auckland, New Zealand, by SPCTRL2 for the 7th of December 2023 at 11:30 am; coordinates (36.8509 S, 174.7645 E); 2.2 cm precipitable water vapour, 1013 mb atmospheric pressure, and 300 DU ozone coverage [27].

The authors in [26] have further extended this work, by classifying observations across 1821 stations across the globe into nine different ocean types: S1–S9 by order of surface Chl-a concentration (Fig. 3). Their dimensionless parameterized equation (5) and respective parameters are shown below and in Table I, respectively, where C_b is the surface chlorophyll concentration; s is the vertical gradient of chlorophyll concentration; ζ is the dimensionless depth normalized for the euphotic depth Z_{eu} in metres; C_{max} is the Chl-a concentration at DCM, which occurs at a depth of ζ_{max}, and $\overline{Chl\text{-}a}_{Z_{eu}}$ is the average Chl-a concentration within the euphotic layer in mg m^{-3}. This can be reconstructed to their dimensioned form $C_c(S,z)$ by using (6) and (7). S5–S8 are only plotted for 110 m due to the Chl-a concentration approaching zero. It should also be noted that S9 cannot be modelled beyond shallow depths due to the value of 's' given is 0 [26].

$$C_{DL}(\zeta) = C_b - s\zeta + C_{max}e^{(-[(\zeta-\zeta_{max})/\Delta\zeta]^2)} \quad (5)$$

$$C_c(\zeta) = C_{DL}(\zeta) \times \overline{Chl\text{-}a}_{Z_{eu}} \quad (6)$$

$$z = \zeta \times Z_{eu} \quad (7)$$

Another parameterized version of these data, for Kameda and Matsumura's equation is presented in Johnson *et al.* [28]

who have then proceeded to apply Haltrin's a single-parameter model based on Chl-a concentrations [29] for the derivation of attenuation subcomponents along the stratified column. This may be a more appropriate approach for estimating IOPs underwater due to its relevance for estimating changing attenuation parameters with depth for mobile UOWC and real-life applicability such as for determining UOWC performance characteristics based on georeferenced satellite information of surface Chl-a content. However, here, the authors have instead determined Chl-a concentrations using (5)–(7) and Table I from [26] before applying Haltrin's equations.

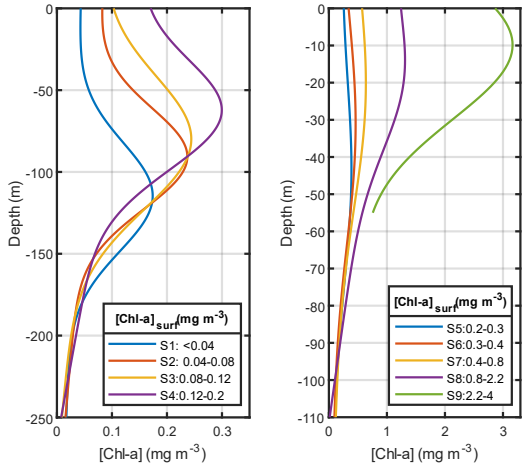

Fig. 3. Reconstructed vertical Chl-a concentration profiles for S1–S9.

TABLE I. DIMENSIONLESS NORMALISED COEFFICIENTS FOR VERTICAL CHLOROPHYLL DISTRIBUTION [26].

Class	C_b	s	C_{max}	ζ_{max}	$\Delta\zeta$	$\overline{\text{Chl-a}}_{Z_{eu}}$	Z_{eu}
S1	0.471	0.135	1.572	0.969	0.393	0.0910	119.1
S2	0.533	0.172	1.194	0.921	0.435	0.151	99.9
S3	0.428	0.138	1.015	0.905	0.630	0.185	91.0
S4	0.57	0.173	0.766	0.814	0.586	0.250	80.2
S5	0.611	0.214	0.676	0.663	0.539	0.338	70.3
S6	0.390	0.109	0.788	0.521	0.681	0.410	63.4
S7	0.569	0.183	0.608	0.452	0.744	0.578	54.4
S8	0.835	0.298	0.382	0.512	0.625	1.206	39.8
S9	0.188	0	0.885	0.378	1.081	2.950	26.1

IV. MATHEMATICAL MODELLING

A. *Haltrin's Single-Parameter IOP Model based on Concentration of Chlorophyll-a*

Haltrin's model has been verified for Chl-a concentrations ranging between 0–12 mg m^{-3} within which are the concentrations of the profiles of stratified water [29]. Prior to this model's application, the depth (z) dependent variation of Chl-a, $C_c(S,z)$, for each classification profile S, needs to be evaluated as given below in subsection B. Thereby, the absorption coefficient $a(S,\lambda,z)$ may be derived with equation (8), where $a_w(\lambda)$ is the pure water absorption coefficient adopted from [30]; $a_c^0(S,\lambda,z)$ is the specific absorption coefficient of Chl-a determined by (9), and the values for empirical constants A and B are available in [31]; C_c^0 is the total reference concentration of Chl-a (1 mg m^{-3}); a_f^0 is the specific absorption coefficient of fulvic acid at 35.959 m^2 mg^{-1}; k_f = 0.0189 nm^{-1}; a_h^0 is the specific absorption coefficient of humic acid at 18.828 m^2 mg^{-1}; k_h = 0.01105 nm^{-1}; and C_f and C_h the concentrations of fulvic and humic acids in mg m^{-3}, calculated using (10) and (11), respectively.

$$a(S,\lambda,z) = a_w(\lambda) + a_c^0(S,\lambda,z)(C_c(S,z)/C_c^0)^{0.602} + a_f^0 C_f(S,z)e^{(-k_f\lambda)} + a_h^0 C_h(S,z)e^{(-k_h\lambda)} \quad (8)$$

$$a_c^0(S,\lambda,z) = A(\lambda)C_c(S,z)^{-B(\lambda)} \quad (9)$$

$$C_f(S,z) = 1.74098C_c(S,z)e^{0.12327(C_c(S,z)/C_c^0)} \quad (10)$$

$$C_h(S,z) = 0.76284C_c(S,z)e^{0.03092(C_c(S,z)/C_c^0)} \quad (11)$$

It should be noted that the above models and those following are computable only for the 400–700 nm wavelength range limited by the reference studies. However, this is sufficient as this covers a full span of the visible spectrum feasible for UOWC due to limitations by attenuation and hardware. This is similar to an optical receiver being fitted with a passband filter of the same optical bandwidth.

The scattering coefficient $b(S,\lambda,z)$ is derived from (12), where $b_w(\lambda)$ is the scattering coefficient of pure water calculated with (13); $b_s^0(\lambda)$ and $b_l^0(\lambda)$ are the specific scattering coefficients of small and large suspended particles, respectively, in m^2 g^{-1}; and $C_s(S,z)$ and $C_l(S,z)$ are the concentrations in g m^{-3} of small and large particles, calculated by (16) and (17), respectively.

$$b(S,\lambda,z) = b_w(\lambda) + b_s^0(\lambda)C_s(S,z) + b_l^0(\lambda)C_l(S,z) \quad (12)$$

$$b_w(\lambda) = 0.005826(400/\lambda)^{4.322} \quad (13)$$

$$b_s^0(\lambda) = 1.151302(400/\lambda)^{1.7} \quad (14)$$

$$b_l^0(\lambda) = 0.341074(400/\lambda)^{0.3} \quad (15)$$

$$C_s(S,z) = 0.01739C_c(S,z)e^{0.11631(C_c(S,z)/C_c^0)} \quad (16)$$

$$C_l(S,z) = 0.76284C_c(S,z)e^{0.03092(C_c(S,z)/C_c^0)} \quad (17)$$

Backscattering may be determined by (18) where B_s (0.039) and B_l (0.00064) are the probabilities of scattering by small and large particles, respectively. Although backscattering is not considered a direct IOP, it is necessary for the evaluation of underwater reflectance, an AOP used in modeling ambient light.

$$b_B(S,\lambda,z) = 0.5b_w(\lambda) + B_s b_s^0(\lambda)C_s(S,z) + B_l b_l^0(\lambda)C_l(S,z) \quad (18)$$

The linear sum of $a(S,\lambda,z)$ and $b(S,\lambda,z)$ as in (1), may be

used to determine the spectral variation in attenuation $c(S,\lambda,z)$ for each profile.

B. Ambient Noise

The downwelling irradiance (E_t) is the sum of all spectral irradiances in W m^{-2} (radiometric) expressed in (19). The background radiance experienced by a receiver of surface area A_r can be derived using (21),

$$E_t = \int E(\lambda)\, d\lambda \tag{19}$$

$$A_r = \pi D^2/4 \tag{20}$$

$$P_{BG}(S,\lambda,z) = \frac{\pi^2 D^2 \Omega^2 T_f \int_\Delta \left(L_{sol}(S,\lambda,z)+L_{bb}(S,\lambda,z)\right) d\lambda}{16} \tag{21}$$

where D and Ω are the diameter and the plane-angle of the field-of-view (FOV) of the receiver in radians, respectively, T_f and Δ are the optical filter transmissivity and bandwidth respectively; L_{sol} is the upwelling solar spectral radiance and L_{bb}, the blackbody radiation of the water body. c_d is the diffuse attenuation coefficient, an AOP, that describes how a background light-field may attenuate in water expressed from IOP by **(22)**. Equation **(4)**, which corresponds to the light intensity at a location may be thereafter adapted for attenuation of downwelling irradiance in a stratified environment using **(23)**, where n is a depth-layer of unit depth in metres and z, is the surface layer**.** Thereby, L_{sol} may be derived for each profile with **(20)**, where R_f is the underwater reflectance that expresses a ratio between downwelling and upwelling irradiances correlated to the backscattering coefficient with **(21)** [32]. L_f is the radiance factor, expressed as the ratio between the radiance observed at an angle of interest (receiver orientation) with respect to the nadir, or looking vertically down. The corresponding values for a horizontal link, and downlink (receiver looking up) were extracted from the sources for clear (S1–S4) and coastal (S5–S9) waters from [22], [21], and [33].

$$c_d(S,\lambda,z) \approx c(S,\lambda,z)/3 \tag{22}$$

$$E_t = \int_\Delta E_0(\lambda) \prod_{n=1}^{z} e^{-c_d(S,\lambda,z_n)}\, d\lambda \tag{23}$$

$$L_{sol}(S,\lambda,z) = E_0(\lambda) R_f(S,\lambda,z) L_f \prod_{n=1}^{z} e^{-c_d(S,\lambda,z_n)}/\pi \tag{24}$$

$$R_f(S,\lambda,z) \approx b_B(S,\lambda,z)/\left(3a(S,\lambda,z)\right) \tag{25}$$

Blackbody radiation is described as the electromagnetic radiation emitted by an object at a particular temperature on the Kelvin scale, idealized for a perfect black object. Its expression is given in **(26)**, where h is the Planck's constant (6.626×10^{-34} Js), v is the speed of light in water (2.253×10^{8} m s^{-1}), k_B is the Boltzmann constant (1.381×10^{-23} J K^{-1}), T is the temperature of the body in Kelvin, and α is the radiance absorption factor (0.5) [11]. Given the underwater environments are about 300 K or lower, much of this radiation available is in the infrared spectrum.

$$L_{bb}(S,\lambda,z) = 2hv^2\alpha/\lambda^5 \left(e^{(hv/k_B T(S,z))} - 1\right) \tag{26}$$

V. Results and Discussion

The downwelling solar spectral irradiance modelled under influence of the stratified water column (Fig. 4a, b) shows the prominence of the blue-amber spectrum with depth, irrespective of the level of clarity of the water. The orange-red spectra seem to be highly attenuated. Results are shown in Fig. 4 for S1, the clearest water and S8, the most turbid water. As expected, the blue-green bandwidth is more prominent in the clear waters of S1 (approx. 300 mW m^{-2} and 25 mW at depths of 100m and 250 m respectively), whereas this shifts to the green-amber region in the highly coastal S8 (approx. 0.25 mW m^{-2} at 100 m depth), both which are significant energies to contribute as noise. However, in the determination of ambient noise power (Fig. 4c - f), the power towards the shorter wavelengths is more significant in the clear waters for receivers placed horizontally and looking vertically up. In the clear water profiles (Fig. 4c – e), the trend of decline for blue-green wavelengths approaching towards the DCM seems to be much greater than beneath the DCM depths, whereas for S8 (Fig. 4d – f), the rate of decline is very high towards the surface, but gradually reduces with increasing depth. Furthermore, the graphs for S8 show higher transmission of the amber spectrum in the upper layers, which gradually shifts to the blue-green spectrum going further down.

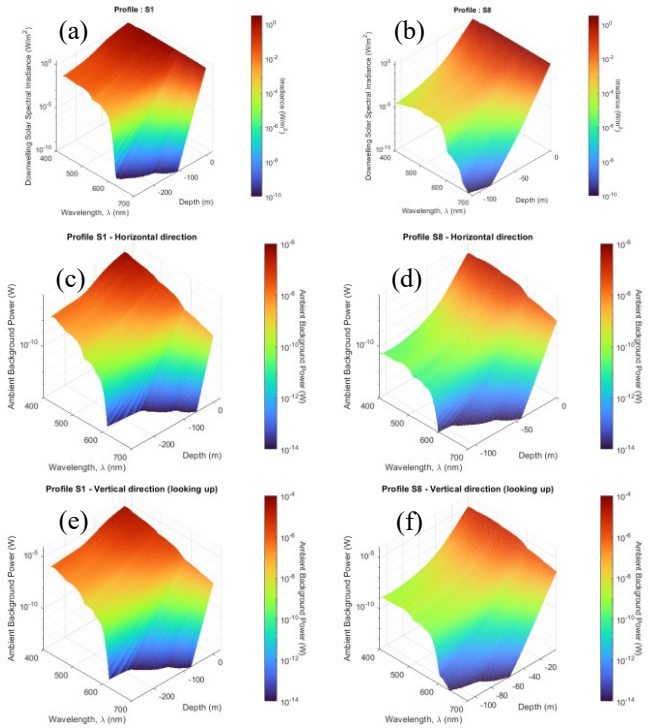

Fig. 4. Downwelling solar spectral irradiance, $E_t(\lambda,z)$ for profiles S1 (a) and S8 (b), and the resultant background power $P_{BG}(\lambda,z)$ for corresponding water profiles (c) and (e), and (d) and (f) in the horizontal and vertical directions respectively.

These observations seem to suggest that blue-green wavelengths from the solar spectrum may have a very high potential to interfere with optical signals of a similar spectral

bandwidth at all depths for clear water profiles, where a longer spectrum such as amber may be preferable for a UOWC link. However, for the S8 profile, the choice of wavelength for UOWC is not so clear cut but may change based on the depth layer the UUV is on. Nevertheless, these results reflect to extent of complexities in UOWCs from an ambient light and attenuation point of view, but would require further study using propagative models, signal-to-noise ratio and bit-error estimates to realistically determine how these influences may affect the link performance based on UOWC parameters such as transmission power, beam divergence and even select signaling schemes.

VI. Conclusion

The UOWC link quality is determined by several time-varying factors: from downwelling sunlight to changing attenuation in inhomogeneous vertical channels, making the determination of optimal link parameters challenging. In this paper, we detailed our modeling of the impact of sunlight as an ambient noise source on UOWC links in eight ocean types stratified vertically in increasing order of turbidity, based on their concentration of Chl-a. The results showed a high penetration of the blue-green solar spectra across all depths, and a preference for amber spectrum by surface layers of the turbid S8 profile that shifted to blue-green spectra as depth increased. As future work, we plan to investigate cross-interactions between UOWC hardware and signaling parameters, and harness them to devise techniques for effective mitigation of ambient light.

References

[1] R. Rayner, C. Jolly, and C. Gouldman, 'Ocean observing and the blue economy', Frontiers in Marine Science, vol. 6, p. 330, 2019.

[2] D. Walsh, 'Exploration and technology—key building blocks for the new blue economy', in Preparing a Workforce for the New Blue Economy, Elsevier, 2021, pp. 3–16.

[3] A. Graham et al., 'Autonomous Marine Systems at Offshore Aquaculture and Energy Sites, 1.20. 002–Final Project Report', 2020.

[4] Y. R. Petillot, G. Antonelli, G. Casalino, and F. Ferreira, 'Underwater robots: From remotely operated vehicles to intervention-autonomous underwater vehicles', IEEE Robotics & Automation Magazine, vol. 26, no. 2, pp. 94–101, 2019.

[5] Y. Yang, Y. Xiao, and T. Li, 'A survey of autonomous underwater vehicle formation: Performance, formation control, and communication capability', IEEE Communications Surveys & Tutorials, vol. 23, no. 2, pp. 815–841, 2021.

[6] J. Connor, B. Champion, and M. A. Joordens, 'Current algorithms, communication methods and designs for underwater swarm robotics: A review', IEEE Sensors Journal, vol. 21, no. 1, pp. 153–169, 2020.

[7] T. J. G. Waduge and M. Joordens, 'Fish robotic research platform for swarms', in 2017 25th International Conference on Systems Engineering (ICSEng), IEEE, 2017, pp. 212–217.

[8] H. Luo, X. Wang, F. Bu, Y. Yang, R. Ruby, and K. Wu, 'Underwater Real-time Video Transmission via Wireless Optical Channels with Swarms of AUVs', IEEE Transactions on Vehicular Technology, vol. 72. no. 11, pp. 14688-14703, 2023.

[9] M. Laranjeira, C. Dune, and V. Hugel, 'Catenary-based visual servoing for tether shape control between underwater vehicles', Ocean Engineering, vol. 200, p. 107018, 2020.

[10] A. Sahoo, S. K. Dwivedy, and P. Robi, 'Advancements in the field of autonomous underwater vehicle', Ocean Engineering, vol. 181, pp. 145–160, 2019.

[11] H. Kaushal and G. Kaddoum, 'Underwater Optical Wireless Communication', IEEE Access, vol. 4, pp. 1518–1547, 2016, doi: 10.1109/ACCESS.2016.2552538.

[12] Y. Li, S. Wang, C. Jin, Y. Zhang, and T. Jiang, 'A survey of underwater magnetic induction communications: Fundamental issues, recent advances, and challenges', IEEE Communications Surveys & Tutorials, vol. 21, no. 3, pp. 2466–2487, 2019.

[13] C.-Y. Li et al., '16 Gb/s PAM4 UWOC system based on 488-nm LD with light injection and optoelectronic feedback techniques', Optics Express, vol. 25, no. 10, pp. 11598–11605, 2017.

[14] T.-C. Wu, Y.-C. Chi, H.-Y. Wang, C.-T. Tsai, and G.-R. Lin, 'Blue laser diode enables underwater communication at 12.4 Gbps', Scientific reports, vol. 7, no. 1, pp. 1–10, 2017.

[15] I.-C. Lu and Y.-L. Liu, '205 Mb/s LED-based underwater optical communication employing OFDM modulation', in 2018 OCEANS-MTS/IEEE Kobe Techno-Oceans (OTO), IEEE, 2018, pp. 1–4.

[16] M. Lanzagorta, 'Underwater communications', Synthesis lectures on communications, vol. 5, no. 2, pp. 1–129, 2012.

[17] C. Gabriel, M.-A. Khalighi, S. Bourennane, P. Léon, and V. Rigaud, 'Monte-Carlo-based channel characterization for underwater optical communication systems', Journal of Optical Communications and Networking, vol. 5, no. 1, pp. 1–12, 2013.

[18] M. G. Solonenko and C. D. Mobley, 'Inherent optical properties of Jerlov water types', Applied optics, vol. 54, no. 17, pp. 5392–5401, 2015.

[19] N. G. Jerlov, 'Optical studies of ocean water', Rept. Swedish Deep-Sea Exped., vol. 3, pp. 1–59, 1951.

[20] J. E. Tyler, 'Radiance distribution as a function of depth in the submarine environment', 1958.

[21] N. K. Hoejerslev and E. Aas, 'Spectral irradiance, radiance, and polarization in blue western Mediterranean waters', in Ocean Optics XIII, SPIE, 1997, pp. 138–147.

[22] S. Q. Duntley, 'Light in the sea', JOSA, vol. 53, no. 2, pp. 214–233, 1963.

[23] R. E. Bird and C. Riordan, 'Simple solar spectral model for direct and diffuse irradiance on horizontal and tilted planes at the earth's surface for cloudless atmospheres', Journal of Applied Meteorology and Climatology, vol. 25, no. 1, pp. 87–97, 1986.

[24] S. D. Miller and R. E. Turner, 'A dynamic lunar spectral irradiance data set for NPOESS/VIIRS day/night band nighttime environmental applications', IEEE Transactions on Geoscience and Remote Sensing, vol. 47, no. 7, pp. 2316–2329, 2009.

[25] T. Kameda and S. Matsumura, 'Chlorophyll biomass off Sanriku, northwestern Pacific, estimated by Ocean Color and Temperature Scanner (OCTS) and a vertical distribution model', Journal of Oceanography, vol. 54, pp. 509–516, 1998.

[26] J. Uitz, H. Claustre, A. Morel, and S. B. Hooker, 'Vertical distribution of phytoplankton communities in open ocean: An assessment based on surface chlorophyll', Journal of Geophysical Research: Oceans, vol. 111, no. C8, 2006.

[27] Solar spectrum calculator. Accessed: Jan. 25, 2023. [Online]. Available: https://www2.pvlighthouse.com.au/calculators/solar%20spectrum%20calculator/solar%20spectrum%20calculator.aspx

[28] L. J. Johnson, R. J. Green, and M. S. Leeson, 'Underwater optical wireless communications: depth dependent variations in attenuation', Applied optics, vol. 52, no. 33, pp. 7867–7873, 2013.

[29] V. I. Haltrin, 'Chlorophyll-based model of seawater optical properties', Applied Optics, vol. 38, no. 33, pp. 6826–6832, 1999.

[30] L. Prieur and S. Sathyendranath, 'An optical classification of coastal and oceanic waters based on the specific spectral absorption curves of phytoplankton pigments, dissolved organic matter, and other particulate materials 1', Limnology and oceanography, vol. 26, no. 4, pp. 671–689, 1981.

[31] R. M. Pope and E. S. Fry, 'Absorption spectrum (380–700 nm) of pure water. II. Integrating cavity measurements', Applied optics, vol. 36, no. 33, pp. 8710–8723, 1997.

[32] J. T. Adams, E. Aas, N. K. Højerslev, and B. Lundgren, 'Comparison of radiance and polarization values observed in the Mediterranean Sea and simulated in a Monte Carlo model', Applied optics, vol. 41, no. 15, pp. 2724–2733, 2002.

[33] E. Aas and N. K. Højerslev, 'Analysis of underwater radiance observations: Apparent optical properties and analytic functions describing the angular radiance distribution', Journal of Geophysical Research: Oceans, vol. 104, no. C4, pp. 8015–8024, 1999.